

Search for baryon and lepton number violating decay $D^\pm \rightarrow n(\bar{n})e^\pm$

M. Ablikim,¹ M. N. Achasov,^{11,b} P. Adlarson,⁷⁰ M. Albrecht,⁴ R. Aliberti,³¹ A. Amoroso,^{69a,69c} M. R. An,³⁵ Q. An,^{66,53} X. H. Bai,⁶¹ Y. Bai,⁵² O. Bakina,³² R. Baldini Ferroli,^{26a} I. Balossino,^{1,27a} Y. Ban,^{42,g} V. Batozskaya,^{1,40} D. Becker,³¹ K. Begzsuren,²⁹ N. Berger,³¹ M. Bertani,^{26a} D. Bettoni,^{27a} F. Bianchi,^{69a,69c} J. Bloms,⁶³ A. Bortone,^{69a,69c} I. Boyko,³² R. A. Briere,⁵ A. Brueggemann,⁶³ H. Cai,⁷¹ X. Cai,^{1,53} A. Calcaterra,^{26a} G. F. Cao,^{1,58} N. Cao,^{1,58} S. A. Cetin,^{57a} J. F. Chang,^{1,53} W. L. Chang,^{1,58} G. Chelkov,^{32,a} C. Chen,³⁹ Chao Chen,⁵⁰ G. Chen,¹ H. S. Chen,^{1,58} M. L. Chen,^{1,53} S. J. Chen,³⁸ S. M. Chen,⁵⁶ T. Chen,¹ X. R. Chen,^{28,58} X. T. Chen,¹ Y. B. Chen,^{1,53} Z. J. Chen,^{23,h} W. S. Cheng,^{69c} S. K. Choi,⁵⁰ X. Chu,³⁹ G. Cibinetto,^{27a} F. Cossio,^{69c} J. J. Cui,⁴⁵ H. L. Dai,^{1,53} J. P. Dai,⁷³ A. Dbeyssi,¹⁷ R. E. de Boer,⁴ D. Dedovich,³² Z. Y. Deng,¹ A. Denig,³¹ I. Denysenko,³² M. Destefanis,^{69a,69c} F. De Mori,^{69a,69c} Y. Ding,³⁶ J. Dong,^{1,53} L. Y. Dong,^{1,58} M. Y. Dong,^{1,53,58} X. Dong,⁷¹ S. X. Du,⁷⁵ P. Egorov,^{32,a} Y. L. Fan,⁷¹ J. Fang,^{1,53} S. S. Fang,^{1,58} W. X. Fang,¹ Y. Fang,¹ R. Farinelli,^{27a} L. Fava,^{69b,69c} F. Feldbauer,⁴ G. Felici,^{26a} C. Q. Feng,^{66,53} J. H. Feng,⁵⁴ K. Fischer,⁶⁴ M. Fritsch,⁴ C. Fritzsche,⁶³ C. D. Fu,¹ H. Gao,⁵⁸ Y. N. Gao,^{42,g} Yang Gao,^{66,53} S. Garbolino,^{69c} I. Garzia,^{27a,27b} P. T. Ge,⁷¹ Z. W. Ge,³⁸ C. Geng,⁵⁴ E. M. Gersabeck,⁶² A. Gilman,⁶⁴ K. Goetzen,¹² L. Gong,³⁶ W. X. Gong,^{1,53} W. Gradl,³¹ M. Greco,^{69a,69c} L. M. Gu,³⁸ M. H. Gu,^{1,53} Y. T. Gu,¹⁴ C. Y. Guan,^{1,58} A. Q. Guo,^{28,58} L. B. Guo,³⁷ R. P. Guo,⁴⁴ Y. P. Guo,^{10,f} A. Guskov,^{32,a} T. T. Han,⁴⁵ W. Y. Han,³⁵ X. Q. Hao,¹⁸ F. A. Harris,⁶⁰ K. K. He,⁵⁰ K. L. He,^{1,58} F. H. Heinsius,⁴ C. H. Heinz,³¹ Y. K. Heng,^{1,53,58} C. Herold,⁵⁵ M. Himmelreich,³¹ G. Y. Hou,^{1,58} Y. R. Hou,⁵⁸ Z. L. Hou,¹ H. M. Hu,^{1,58} J. F. Hu,^{51,i} T. Hu,^{1,53,58} Y. Hu,¹ G. S. Huang,^{66,53} K. X. Huang,⁵⁴ L. Q. Huang,⁶⁷ L. Q. Huang,^{28,58} X. T. Huang,⁴⁵ Y. P. Huang,¹ Z. Huang,^{42,g} T. Hussain,⁶⁸ N. Hüsken,^{25,31} W. Imoehl,²⁵ M. Irshad,^{66,53} J. Jackson,²⁵ S. Jaeger,⁴ S. Janchiv,²⁹ E. Jang,⁵⁰ J. H. Jeong,⁵⁰ Q. Ji,¹ Q. P. Ji,¹⁸ X. B. Ji,^{1,58} X. L. Ji,^{1,53} Y. Y. Ji,⁴⁵ Z. K. Jia,^{66,53} H. B. Jiang,⁴⁵ S. S. Jiang,³⁵ X. S. Jiang,^{1,53,58} Y. Jiang,⁵⁸ J. B. Jiao,⁴⁵ Z. Jiao,²¹ S. Jin,³⁸ Y. Jin,⁶¹ M. Q. Jing,^{1,58} T. Johansson,⁷⁰ N. Kalantar-Nayestanaki,⁵⁹ X. S. Kang,³⁶ R. Kappert,⁵⁹ M. Kavatsyuk,⁵⁹ B. C. Ke,⁷⁵ I. K. Keshk,⁴ A. Khoukaz,⁶³ P. Kiese,³¹ R. Kiuchi,¹ R. Kliemt,¹² L. Koch,³³ O. B. Kolcu,^{57a} B. Kopf,⁴ M. Kuemmel,⁴ M. Kuessner,⁴ A. Kupsc,^{40,70} W. Kühn,³³ J. J. Lane,⁶² J. S. Lange,³³ P. Larin,¹⁷ A. Lavania,²⁴ L. Lavezzi,^{69a,69c} Z. H. Lei,^{66,53} H. Leithoff,³¹ M. Lellmann,³¹ T. Lenz,³¹ C. Li,⁴³ C. Li,³⁹ C. H. Li,³⁵ Cheng Li,^{66,53} D. M. Li,⁷⁵ F. Li,^{1,53} G. Li,¹ H. Li,⁴⁷ H. Li,^{66,53} H. B. Li,^{1,58} H. J. Li,¹⁸ H. N. Li,^{51,i} J. Q. Li,⁴ J. S. Li,⁵⁴ J. W. Li,⁴⁵ Ke Li,¹ L. J. Li,¹ L. K. Li,¹ Lei Li,³ M. H. Li,³⁹ P. R. Li,^{34,j,k} S. X. Li,¹⁰ S. Y. Li,⁵⁶ T. Li,⁴⁵ W. D. Li,^{1,58} W. G. Li,¹ X. H. Li,^{66,53} X. L. Li,⁴⁵ Xiaoyu Li,^{1,58} H. Liang,^{66,53} H. Liang,^{1,58} H. Liang,³⁰ Y. F. Liang,⁴⁹ Y. T. Liang,^{28,58} G. R. Liao,¹³ L. Z. Liao,⁴⁵ J. Libby,²⁴ A. Limphirat,⁵⁵ C. X. Lin,⁵⁴ D. X. Lin,^{28,58} T. Lin,¹ B. J. Liu,¹ C. X. Liu,¹ D. Liu,^{17,66} F. H. Liu,⁴⁸ Fang Liu,¹ Feng Liu,⁶ G. M. Liu,^{51,i} H. Liu,^{34,j,k} H. B. Liu,¹⁴ H. M. Liu,^{1,58} Huanhuan Liu,¹ Huihui Liu,¹⁹ J. B. Liu,^{66,53} J. L. Liu,⁶⁷ J. Y. Liu,^{1,58} K. Liu,¹ K. Y. Liu,³⁶ Ke Liu,²⁰ L. Liu,^{66,53} Lu Liu,³⁹ M. H. Liu,^{10,f} P. L. Liu,¹ Q. Liu,⁵⁸ S. B. Liu,^{66,53} T. Liu,^{10,f} W. K. Liu,³⁹ W. M. Liu,^{66,53} X. Liu,^{34,j,k} Y. Liu,^{34,j,k} Y. B. Liu,³⁹ Z. A. Liu,^{1,53,58} Z. Q. Liu,⁴⁵ X. C. Lou,^{1,53,58} F. X. Lu,⁵⁴ H. J. Lu,²¹ J. G. Lu,^{1,53} X. L. Lu,¹ Y. Lu,⁷ Y. P. Lu,^{1,53} Z. H. Lu,¹ C. L. Luo,³⁷ M. X. Luo,⁷⁴ T. Luo,^{10,f} X. L. Luo,^{1,53} X. R. Lyu,⁵⁸ Y. F. Lyu,³⁹ F. C. Ma,³⁶ H. L. Ma,¹ L. L. Ma,⁴⁵ M. M. Ma,^{1,58} Q. M. Ma,¹ R. Q. Ma,^{1,58} R. T. Ma,⁵⁸ X. Y. Ma,^{1,53} Y. Ma,^{42,g} F. E. Maas,¹⁷ M. Maggiora,^{69a,69c} S. Maldaner,⁴ S. Malde,⁶⁴ Q. A. Malik,⁶⁸ A. Mangoni,^{26b} Y. J. Mao,^{42,g,g} Z. P. Mao,¹ S. Marcello,^{69a,69c} Z. X. Meng,⁶¹ J. G. Messchendorp,^{59,12} G. Mezzadri,^{1,27a} H. Miao,¹ T. J. Min,³⁸ R. E. Mitchell,²⁵ X. H. Mo,^{1,53,58} N. Yu. Muchnoi,^{11,b} Y. Nefedov,³² F. Nerling,^{17,d} I. B. Nikolaev,¹¹ Z. Ning,^{1,53} S. Nisar,^{9,1} Y. Niu,⁴⁵ S. L. Olsen,⁵⁸ Q. Ouyang,^{1,53,58} S. Pacetti,^{26b,26c} X. Pan,^{10,f} Y. Pan,⁵² A. Pathak,¹ A. Pathak,³⁰ M. Pelizaeus,⁴ H. P. Peng,^{66,53} K. Peters,^{12,d} J. Pettersson,⁷⁰ J. L. Ping,³⁷ R. G. Ping,^{1,58} S. Plura,³¹ S. Pogodin,³² V. Prasad,^{66,53} F. Z. Qi,¹ H. Qi,^{66,53} H. R. Qi,⁵⁶ M. Qi,³⁸ T. Y. Qi,^{10,f} S. Qian,^{1,53} W. B. Qian,⁵⁸ Z. Qian,⁵⁴ C. F. Qiao,⁵⁸ J. J. Qin,⁶⁷ L. Q. Qin,¹³ X. P. Qin,^{10,f} X. S. Qin,⁴⁵ Z. H. Qin,^{1,53} J. F. Qiu,¹ S. Q. Qu,³⁹ S. Q. Qu,⁵⁶ K. H. Rashid,⁶⁸ C. F. Redmer,³¹ K. J. Ren,³⁵ A. Rivetti,^{69c} V. Rodin,⁵⁹ M. Rolo,^{69c} G. Rong,^{1,58} Ch. Rosner,¹⁷ S. N. Ruan,³⁹ H. S. Sang,⁶⁶ A. Sarantsev,^{32,c} Y. Schelhaas,³¹ C. Schnier,⁴ K. Schönning,⁷⁰ M. Scodreggio,^{27a,27b} K. Y. Shan,^{10,f} W. Shan,²² X. Y. Shan,^{66,53} J. F. Shangguan,⁵⁰ L. G. Shao,^{1,58} M. Shao,^{66,53} C. P. Shen,^{10,f} H. F. Shen,^{1,58} X. Y. Shen,^{1,58} B. A. Shi,⁵⁸ H. C. Shi,^{66,53} J. Y. Shi,¹ Q. Q. Shi,⁵⁰ R. S. Shi,^{1,58} X. Shi,^{1,53} X. D. Shi,^{66,53} J. J. Song,¹⁸ W. M. Song,^{1,30} Y. X. Song,^{42,g} S. Sosio,^{69a,69c} S. Spataro,^{69a,69c} F. Stieler,³¹ K. X. Su,⁷¹ P. P. Su,⁵⁰ Y. J. Su,⁵⁸ G. X. Sun,¹ H. Sun,⁵⁸ H. K. Sun,¹ J. F. Sun,¹⁸ L. Sun,⁷¹ S. S. Sun,^{1,58} T. Sun,^{1,58} W. Y. Sun,³⁰ X. Sun,^{23,h} Y. J. Sun,^{66,53} Y. Z. Sun,¹ Z. T. Sun,⁴⁵ Y. H. Tan,⁷¹ Y. X. Tan,^{66,53} C. J. Tang,⁴⁹ G. Y. Tang,¹ J. Tang,⁵⁴ L. Y. Tao,⁶⁷ Q. T. Tao,^{23,h} M. Tat,⁶⁴ J. X. Teng,^{66,53} V. Thoren,⁷⁰ W. H. Tian,⁴⁷ Y. Tian,^{28,58} I. Uman,^{57b} B. Wang,¹ B. L. Wang,⁵⁸ C. W. Wang,³⁸ D. Y. Wang,^{42,g} F. Wang,⁶⁷ H. J. Wang,^{34,j,k} H. P. Wang,^{1,58} K. Wang,^{1,53} L. L. Wang,¹ M. Wang,⁴⁵ M. Z. Wang,^{42,g} Meng Wang,^{1,58} S. Wang,¹³ S. Wang,^{10,f} T. Wang,^{10,f} T. J. Wang,³⁹ W. Wang,⁵⁴ W. H. Wang,⁷¹ W. P. Wang,^{66,53} X. Wang,^{42,g} X. F. Wang,^{34,j,k} X. L. Wang,^{10,f} Y. D. Wang,⁴¹ Y. F. Wang,^{1,53,58} Y. H. Wang,⁴³ Y. Q. Wang,¹ Yaqian Wang,^{1,16} Y. Wang,⁵⁶ Z. Wang,^{1,53} Z. Y. Wang,^{1,58} Ziyi Wang,⁵⁸ D. H. Wei,¹³ F. Weidner,⁶³ S. P. Wen,¹ D. J. White,⁶² U. Wiedner,⁴ G. Wilkinson,⁶⁴ M. Wolke,⁷⁰ L. Wollenberg,⁴ J. F. Wu,^{1,58} L. H. Wu,¹ L. J. Wu,^{1,58} X. Wu,^{10,f} X. H. Wu,³⁰ Y. Wu,⁶⁶ Z. Wu,^{1,53} L. Xia,^{66,53} T. Xiang,^{42,g} D. Xiao,^{34,j,k} G. Y. Xiao,³⁸ H. Xiao,^{10,f}

S. Y. Xiao,¹ Y. L. Xiao,^{10,f} Z. J. Xiao,³⁷ C. Xie,³⁸ X. H. Xie,^{42,g} Y. Xie,⁴⁵ Y. G. Xie,^{1,53} Y. H. Xie,⁶ Z. P. Xie,^{66,53}
 T. Y. Xing,^{1,58} C. F. Xu,¹ C. J. Xu,⁵⁴ G. F. Xu,¹ H. Y. Xu,⁶¹ Q. J. Xu,¹⁵ X. P. Xu,⁵⁰ Y. C. Xu,⁵⁸ Z. P. Xu,³⁸ F. Yan,^{10,f} L. Yan,^{10,f}
 W. B. Yan,^{66,53} W. C. Yan,⁷⁵ H. J. Yang,^{46,e} H. L. Yang,³⁰ H. X. Yang,¹ L. Yang,⁴⁷ S. L. Yang,⁵⁸ Tao Yang,¹ Y. F. Yang,³⁹
 Y. X. Yang,^{1,58} Yifan Yang,^{1,58} M. Ye,^{1,53} M. H. Ye,⁸ J. H. Yin,¹ Z. Y. You,⁵⁴ B. X. Yu,^{1,53,58} C. X. Yu,³⁹ G. Yu,^{1,58} T. Yu,⁶⁷
 X. D. Yu,^{42,g} C. Z. Yuan,^{1,58} L. Yuan,² S. C. Yuan,¹ X. Q. Yuan,¹ Y. Yuan,^{1,58} Z. Y. Yuan,⁵⁴ C. X. Yue,³⁵ A. A. Zafar,⁶⁸
 F. R. Zeng,⁴⁵ X. Zeng,⁶ Y. Zeng,^{23,h} Y. H. Zhan,⁵⁴ A. Q. Zhang,¹ B. L. Zhang,¹ B. X. Zhang,¹ D. H. Zhang,³⁹ G. Y. Zhang,¹⁸
 H. Zhang,⁶⁶ H. H. Zhang,⁵⁴ H. H. Zhang,³⁰ H. Y. Zhang,^{1,53} J. L. Zhang,⁷² J. Q. Zhang,³⁷ J. W. Zhang,^{1,53,58} J. X. Zhang,^{34,j,k}
 J. Y. Zhang,¹ J. Z. Zhang,^{1,58} Jianyu Zhang,^{1,58} Jiawei Zhang,^{1,58} L. M. Zhang,⁵⁶ L. Q. Zhang,⁵⁴ Lei Zhang,³⁸ P. Zhang,¹
 Q. Y. Zhang,^{35,75} Shuihan Zhang,^{1,58} Shulei Zhang,^{23,h} X. D. Zhang,⁴¹ X. M. Zhang,¹ X. Y. Zhang,⁴⁵ X. Y. Zhang,⁵⁰
 Y. Zhang,⁶⁴ Y. T. Zhang,⁷⁵ Y. H. Zhang,^{1,53} Yan Zhang,^{66,53} Yao Zhang,¹ Z. H. Zhang,¹ Z. Y. Zhang,⁷¹ Z. Y. Zhang,³⁹
 G. Zhao,¹ J. Zhao,³⁵ J. Y. Zhao,^{1,58} J. Z. Zhao,^{1,53} Lei Zhao,^{66,53} Ling Zhao,¹ M. G. Zhao,³⁹ Q. Zhao,¹ S. J. Zhao,⁷⁵
 Y. B. Zhao,^{1,53} Y. X. Zhao,^{28,58} Z. G. Zhao,^{66,53} A. Zhemchugov,^{32,a} B. Zheng,⁶⁷ J. P. Zheng,^{1,53} Y. H. Zheng,⁵⁸ B. Zhong,³⁷
 C. Zhong,⁶⁷ X. Zhong,⁵⁴ H. Zhou,⁴⁵ L. P. Zhou,^{1,58} X. Zhou,⁷¹ X. K. Zhou,⁵⁸ X. R. Zhou,^{66,53} X. Y. Zhou,³⁵ Y. Z. Zhou,^{10,f}
 J. Zhu,³⁹ K. Zhu,¹ K. J. Zhu,^{1,53,58} L. X. Zhu,⁵⁸ S. H. Zhu,⁶⁵ S. Q. Zhu,³⁸ T. J. Zhu,⁷² W. J. Zhu,^{10,f} Y. C. Zhu,^{66,53}
 Z. A. Zhu,^{1,58} B. S. Zou,¹ and J. H. Zou¹

(BESIII Collaboration)

¹*Institute of High Energy Physics, Beijing 100049, People's Republic of China*²*Beihang University, Beijing 100191, People's Republic of China*³*Beijing Institute of Petrochemical Technology, Beijing 102617, People's Republic of China*⁴*Bochum Ruhr-University, D-44780 Bochum, Germany*⁵*Carnegie Mellon University, Pittsburgh, Pennsylvania 15213, USA*⁶*Central China Normal University, Wuhan 430079, People's Republic of China*⁷*Central South University, Changsha 410083, People's Republic of China*⁸*China Center of Advanced Science and Technology, Beijing 100190, People's Republic of China*⁹*COMSATS University Islamabad, Lahore Campus,**Defence Road, Off Raiwind Road, 54000 Lahore, Pakistan*¹⁰*Fudan University, Shanghai 200433, People's Republic of China*¹¹*G.I. Budker Institute of Nuclear Physics SB RAS (BINP), Novosibirsk 630090, Russia*¹²*GSI Helmholtzcentre for Heavy Ion Research GmbH, D-64291 Darmstadt, Germany*¹³*Guangxi Normal University, Guilin 541004, People's Republic of China*¹⁴*Guangxi University, Nanning 530004, People's Republic of China*¹⁵*Hangzhou Normal University, Hangzhou 310036, People's Republic of China*¹⁶*Hebei University, Baoding 071002, People's Republic of China*¹⁷*Helmholtz Institute Mainz, Staudinger Weg 18, D-55099 Mainz, Germany*¹⁸*Henan Normal University, Xinxiang 453007, People's Republic of China*¹⁹*Henan University of Science and Technology, Luoyang 471003, People's Republic of China*²⁰*Henan University of Technology, Zhengzhou 450001, People's Republic of China*²¹*Huangshan College, Huangshan 245000, People's Republic of China*²²*Hunan Normal University, Changsha 410081, People's Republic of China*²³*Hunan University, Changsha 410082, People's Republic of China*²⁴*Indian Institute of Technology Madras, Chennai 600036, India*²⁵*Indiana University, Bloomington, Indiana 47405, USA*^{26a}*INFN Laboratori Nazionali di Frascati, I-00044 Frascati, Italy*^{26b}*INFN Sezione di Perugia, I-06100, Perugia, Italy*^{26c}*University of Perugia, I-06100 Perugia, Italy*^{27a}*INFN Sezione di Ferrara, I-44122, Ferrara, Italy*^{27b}*University of Ferrara, I-44122 Ferrara, Italy*²⁸*Institute of Modern Physics, Lanzhou 730000, People's Republic of China*²⁹*Institute of Physics and Technology, Peace Avenue 54B, Ulaanbaatar 13330, Mongolia*³⁰*Jilin University, Changchun 130012, People's Republic of China*³¹*Johannes Gutenberg University of Mainz, Johann-Joachim-Becher-Weg 45, D-55099 Mainz, Germany*³²*Joint Institute for Nuclear Research, 141980 Dubna, Moscow region, Russia*³³*Justus-Liebig-Universitaet Giessen, II. Physikalisches Institut,**Heinrich-Buff-Ring 16, D-35392 Giessen, Germany*³⁴*Lanzhou University, Lanzhou 730000, People's Republic of China*³⁵*Liaoning Normal University, Dalian 116029, People's Republic of China*

- ³⁶Liaoning University, Shenyang 110036, People's Republic of China
³⁷Nanjing Normal University, Nanjing 210023, People's Republic of China
³⁸Nanjing University, Nanjing 210093, People's Republic of China
³⁹Nankai University, Tianjin 300071, People's Republic of China
⁴⁰National Centre for Nuclear Research, Warsaw 02-093, Poland
⁴¹North China Electric Power University, Beijing 102206, People's Republic of China
⁴²Peking University, Beijing 100871, People's Republic of China
⁴³Qufu Normal University, Qufu 273165, People's Republic of China
⁴⁴Shandong Normal University, Jinan 250014, People's Republic of China
⁴⁵Shandong University, Jinan 250100, People's Republic of China
⁴⁶Shanghai Jiao Tong University, Shanghai 200240, People's Republic of China
⁴⁷Shanxi Normal University, Linfen 041004, People's Republic of China
⁴⁸Shanxi University, Taiyuan 030006, People's Republic of China
⁴⁹Sichuan University, Chengdu 610064, People's Republic of China
⁵⁰Soochow University, Suzhou 215006, People's Republic of China
⁵¹South China Normal University, Guangzhou 510006, People's Republic of China
⁵²Southeast University, Nanjing 211100, People's Republic of China
⁵³State Key Laboratory of Particle Detection and Electronics,
Beijing 100049, Hefei 230026, People's Republic of China
⁵⁴Sun Yat-Sen University, Guangzhou 510275, People's Republic of China
⁵⁵Suranaree University of Technology, University Avenue 111, Nakhon Ratchasima 30000, Thailand
⁵⁶Tsinghua University, Beijing 100084, People's Republic of China
^{57a}Turkish Accelerator Center Particle Factory Group, Istinye University, 34010, Istanbul, Turkey
^{57b}Near East University, Nicosia, North Cyprus, Mersin 10, Turkey
⁵⁸University of Chinese Academy of Sciences, Beijing 100049, People's Republic of China
⁵⁹University of Groningen, NL-9747 AA Groningen, The Netherlands
⁶⁰University of Hawaii, Honolulu, Hawaii 96822, USA
⁶¹University of Jinan, Jinan 250022, People's Republic of China
⁶²University of Manchester, Oxford Road, Manchester, M13 9PL, United Kingdom
⁶³University of Muenster, Wilhelm-Klemm-Strasse 9, 48149 Muenster, Germany
⁶⁴University of Oxford, Keble Road, Oxford OX13RH, United Kingdom
⁶⁵University of Science and Technology Liaoning, Anshan 114051, People's Republic of China
⁶⁶University of Science and Technology of China, Hefei 230026, People's Republic of China
⁶⁷University of South China, Hengyang 421001, People's Republic of China
⁶⁸University of the Punjab, Lahore-54590, Pakistan
^{69a}University of Turin and INFN, University of Turin, I-10125, Turin, Italy
^{69b}University of Eastern Piedmont, I-15121, Alessandria, Italy
^{69c}INFN, I-10125, Turin, Italy
⁷⁰Uppsala University, Box 516, SE-75120 Uppsala, Sweden
⁷¹Wuhan University, Wuhan 430072, People's Republic of China
⁷²Xinyang Normal University, Xinyang 464000, People's Republic of China
⁷³Yunnan University, Kunming 650500, People's Republic of China
⁷⁴Zhejiang University, Hangzhou 310027, People's Republic of China
⁷⁵Zhengzhou University, Zhengzhou 450001, People's Republic of China

^aAlso at the Moscow Institute of Physics and Technology, Moscow 141700, Russia.

^bAlso at the Novosibirsk State University, Novosibirsk, 630090, Russia.

^cAlso at the NRC "Kurchatov Institute", PNPI, 188300, Gatchina, Russia.

^dAlso at Goethe University Frankfurt, 60323 Frankfurt am Main, Germany.

^eAlso at Key Laboratory for Particle Physics, Astrophysics and Cosmology, Ministry of Education; Shanghai Key Laboratory for Particle Physics and Cosmology; Institute of Nuclear and Particle Physics, Shanghai 200240, People's Republic of China.

^fAlso at Key Laboratory of Nuclear Physics and Ion-beam Application (MOE) and Institute of Modern Physics, Fudan University, Shanghai 200443, People's Republic of China.

^gAlso at State Key Laboratory of Nuclear Physics and Technology, Peking University, Beijing 100871, People's Republic of China.


^hAlso at School of Physics and Electronics, Hunan University, Changsha 410082, China.

ⁱAlso at Guangdong Provincial Key Laboratory of Nuclear Science, Institute of Quantum Matter, South China Normal University, Guangzhou 510006, China.

^jAlso at Frontiers Science Center for Rare Isotopes, Lanzhou University, Lanzhou 730000, People's Republic of China.

^kAlso at Lanzhou Center for Theoretical Physics, Lanzhou University, Lanzhou 730000, People's Republic of China.

^lAlso at the Department of Mathematical Sciences, IBA, Karachi, Pakistan.

 (Received 14 September 2022; accepted 29 November 2022; published 26 December 2022)

Using a data set of electron-positron collisions corresponding to an integrated luminosity of 293 fb^{-1} taken with the BESIII detector at a center-of-mass energy of 3.773 GeV , a search for the baryon (B) and lepton (L) number violating decays $D^\pm \rightarrow n(\bar{n})e^\pm$ is performed. No signal is observed and the upper limits on the branching fractions at the 90% confidence level are set to be 1.43×10^{-5} for the decays $D^{+(-)} \rightarrow \bar{n}(n)e^{+(-)}$ with $\Delta|B - L| = 0$, and 2.91×10^{-5} for the decays $D^{+(-)} \rightarrow n(\bar{n})e^{+(-)}$ with $\Delta|B - L| = 2$, where $\Delta|B - L|$ denotes the change in the difference between baryon and lepton numbers.

DOI: [10.1103/PhysRevD.106.112009](https://doi.org/10.1103/PhysRevD.106.112009)

I. INTRODUCTION

The search for new physics beyond the Standard Model (SM) is one of the major goals of particle physics. The matter-antimatter asymmetry of the Universe is one prominent observations that cannot be explained within the SM, and as such is a serious challenge to our understanding of nature. This asymmetry suggests the existence of baryon number violation (BNV) [1]. While proton decay has been searched for decades but not yet observed, the search for decays of heavy mesons and baryons that are forbidden in the SM can provide an alternative probe to search for BNV. In most grand unified theories (GUTs) [2–6] and some SM extension models [7,8], baryon-number and lepton-number violation (LNV) is allowed, but the difference of baryon and lepton numbers is conserved ($\Delta|B - L| = 0$). Dimension-six operators allow processes with $\Delta|B - L| = 0$ to proceed, mediated by heavy gauge bosons X with charge $\frac{4}{3}$ or Y with charge $\frac{1}{3}$, as shown in Feynman diagrams in Figs. 1(a) and 1(b) for D meson decays. Furthermore, there is another BNV process possible under dimension-seven operators, mediated by an elementary scalar field ϕ , as shown in Fig. 1(c). In this process, the difference of baryon and lepton number is changed by 2 units ($\Delta|B - L| = 2$). Reference [9] argues that the decay amplitudes of these two kinds of BNV processes are expected to be of comparable strength. Thus, experimental searches for these BNV decays probe new physics effects and test different models beyond the SM.

The CLEO, BABAR, and CLAS experiments searched for BNV processes in D , B meson, and hyperon decays [10–12], respectively, without finding evidence of a signal. Upper limits (ULs) were set on the decay branching fractions in the range of $10^{-5} \sim 10^{-8}$ at the 90% confidence level (C.L.). Recently, the BESIII experiment searched for D^+ meson decays to a hyperon and an electron, i.e.,

$D^+ \rightarrow \bar{\Lambda}(\bar{\Sigma}^0)e^+$ with $\Delta(B - L) = 0$ and $D^+ \rightarrow \Lambda(\Sigma^0)e^+$ with $\Delta(B - L) = 2$. No signal was found and ULs of around 10^{-6} were set on the decay branching fractions at the 90% C.L. [13]. It is natural to extend the search to D^+ meson decays to a (anti)neutron and electron pair. A higher generation SUSY model [14] predicts the branching fraction of $D^0 \rightarrow \bar{p}\ell^+$ ($\ell^+ = e^+, \mu^+$) to be less than 4.0×10^{-39} , thus the decay $D^+ \rightarrow \bar{n}\ell^+$ is also expected to be of a comparable magnitude because it differs only by the change of a spectator quark.

In this paper, we report the first search for the BNV process $D^{+(-)} \rightarrow \bar{n}(n)e^{+(-)}$ with $\Delta|B - L| = 0$, and $D^{+(-)} \rightarrow n(\bar{n})e^{+(-)}$ with $\Delta|B - L| = 2$ by using 2.93 fb^{-1} of electron-positron collision data taken at a center-of-mass energy of $\sqrt{s} = 3.773 \text{ GeV}$. Throughout this paper, the presence of charge-conjugated processes are implied unless explicitly stated otherwise.

II. BESIII DETECTOR AND MONTE CARLO SIMULATION

The BESIII detector is a magnetic spectrometer [15] located at the Beijing Electron Positron Collider (BEPCII) [16]. The cylindrical core of the BESIII detector consists of a helium-based multilayer drift chamber (MDC), a plastic scintillator time-of-flight system (TOF), and a CsI(Tl) electromagnetic calorimeter (EMC), which are all enclosed

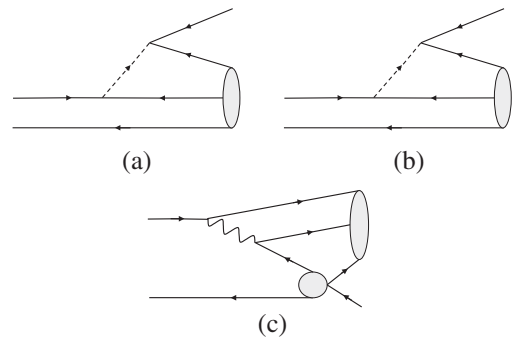


FIG. 1. Feynman diagrams for $D^+ \rightarrow \bar{n}e^+$ with heavy gauge bosons X (a) and Y (b), and $D^+ \rightarrow ne^+$ with elementary scalar fields ϕ (c).

in a superconducting solenoidal magnet providing a 1.0 T magnetic field. The solenoid is supported by an octagonal flux-return yoke with resistive plate counter muon identifier modules interleaved with steel. The acceptance of charged particles and photons is 93% over 4π solid angle. The charged-particle momentum resolution at 1 GeV/ c is 0.5%, and the specific energy loss (dE/dx) resolution is 6% for the electrons from Bhabha scattering. The EMC measures photon energies with a resolution of 2.5% (5%) at 1 GeV in the barrel (end cap) region. The TOF measures flight time of charged particle with a resolution 68 ps in the barrel region, and 110 ps in the end cap region when the data sets in this analysis were collected.

Monte Carlo (MC) simulation samples, generated with a GEANT4-based [17] package [18], including the geometric and material description of the BESIII detector, are used to determine the detection efficiency, optimize the selection criteria and estimate the backgrounds. The analysis is performed in the framework of the BESIII Offline Software System [19], which takes care of the detector calibration, event reconstruction and data storage. The simulation includes the beam energy spread and initial state radiation (ISR) in the e^+e^- annihilations modeled with the generator KKMC [20]. The inclusive MC samples contain the production of $D\bar{D}$ pairs, the non- $D\bar{D}$ decays of the $\psi(3770)$, the ISR production of the J/ψ and $\psi(3686)$ states, and continuum processes, in which the known decay modes are modeled with EVTGEN [21] using branching fractions taken from the Particle Data Group (PDG) [22], and the remaining unknown decays from charmonium states are modeled with LUNDCHARM [23,24]. The final-state radiation from charged particles is incorporated using PHOTOS [25]. In the signal MC sample, D^+D^- pairs are generated by the VSS model from EVTGEN [21] and the signal process is generated with a uniform momentum distribution in the phase space (PHSP) according to the conservation of angular momentum.

III. DATA ANALYSIS

A. Analysis method

At $\sqrt{s} = 3.773$ GeV, D^\pm mesons are produced in pairs without the presence of any additional fragmentation particles. This property provides an ideal environment for investigating D^\pm meson decays with a double-tag (DT) method [26]. In this approach, the single-tag (ST) D^\pm meson is reconstructed in six hadronic decay modes $D^+ \rightarrow K^-\pi^+\pi^+$, $D^+ \rightarrow K^-\pi^+\pi^+\pi^0$, $D^+ \rightarrow K_S^0\pi^+$, $D^+ \rightarrow K_S^0\pi^+\pi^0$, $D^+ \rightarrow K_S^0\pi^+\pi^+\pi^-$ and $D^+ \rightarrow K^+\pi^-\pi^+$, all of which have relatively large branching fractions and low background contamination. The DTs are then formed by reconstructing the other charm meson in the event in its decay to the signal mode. The decay branching fractions of the four signal modes ($D^{+(-)} \rightarrow \bar{n}(n)e^{+(-)}$ and $D^{+(-)} \rightarrow n(\bar{n})e^{+(-)}$) are determined independently by

$$\mathcal{B}_{\text{sig}} = N_{\text{DT}} / (N_{\text{ST}}^{\text{tot}} \cdot \epsilon_{\text{sig}}), \quad (1)$$

where $N_{\text{ST}}^{\text{tot}}$ and N_{DT} are respectively the yields of ST and DT events in data summed over all ST decay modes. The effective signal detection efficiency in the presence of the ST D^\pm meson is calculated by $\epsilon_{\text{sig}} = \sum_i [(\epsilon_{\text{DT}}^i \cdot N_{\text{ST}}^i) / (\epsilon_{\text{ST}}^i \cdot N_{\text{ST}}^{\text{tot}})]$, where ϵ_{ST}^i and ϵ_{DT}^i are the corresponding detection efficiencies of the ST and DT method for the i^{th} tag mode, respectively, and i sums over all ST decay modes.

To avoid possible bias, a blind analysis technique is performed in which the data in the interesting phase space region are viewed only after the analysis strategy is validated with MC simulation or data in the control region and then fixed.

B. Event selection

Charged particles, including kaon, pion and electron/positron candidates, are reconstructed from the hit information in the MDC. The charged tracks, apart from in the case of pions from the decays of candidate K_S^0 mesons, are required to have a distance of closest approach to the interaction point (IP) within ± 10 cm in the beam direction and 1 cm in the plane perpendicular to the beam. The polar angle θ of charged tracks with respect to the z -axis of the MDC must satisfy $|\cos\theta| < 0.93$. Particle identification (PID), based on the information from the dE/dx and TOF measurements, is applied to the charged tracks and the CLs for the kaon and pion hypotheses ($\text{CL}_{K,\pi}$) are calculated. A kaon is identified by requiring $\text{CL}_K > \text{CL}_\pi$, and a pion by requiring $\text{CL}_\pi > \text{CL}_K$. To identify electrons, the deposited energy in the EMC is utilized, in addition to the dE/dx and TOF information, and the CLs are calculated for the electron, pion, kaon, and proton hypotheses ($\text{CL}_{e,\pi,K,p}$), individually. An electron is identified by requiring $\text{CL}_e / (\text{CL}_e + \text{CL}_\pi + \text{CL}_K + \text{CL}_p) > 0.8$.

Photon candidates are reconstructed from EMC showers and are required to have energy greater than 25 MeV in the barrel region ($|\cos\theta| < 0.8$), and 50 MeV in the end-cap region ($0.86 < |\cos\theta| < 0.92$). To suppress showers from electronic noise and those unrelated to the event under analysis, the EMC shower time is required to be within 700 ns of the start time of the event. The minimum opening angle between the photon candidate and all charged tracks is required to be greater than 10° to avoid contamination from charged tracks showering in the EMC detector. The π^0 candidates are reconstructed from photon pairs by requiring the invariant mass ($M_{\gamma\gamma}$) to be in the range (0.115, 0.150) GeV/ c^2 . To improve the kinematic resolution, a kinematic fit constraining $M_{\gamma\gamma}$ to the nominal π^0 mass [22] is applied to the π^0 candidate. The kinematic variables after the kinematic fit are used in the subsequent analysis.

The K_S^0 candidates are reconstructed from two charged tracks with opposite charges, polar angle in the range

$|\cos\theta| < 0.93$ and points of closest approach to the IP within ± 20 cm along the beam direction. No requirement on the distance of closest approach in the plane perpendicular to the z direction is applied. A vertex fit is performed on the two tracks on the assumption that they are pions from a common decay point. A further secondary vertex fit, which constrains the K_S^0 to come from the beamspot, is applied to suppress background with the requirement $L/\sigma_L > 2$, where L is the decay length, defined as the distance between the primary and secondary vertexes, and σ_L is the corresponding resolution. The invariant mass ($M_{\pi\pi}$) must satisfy $|M_{\pi\pi} - M_{K_S^0}| < 0.012 \text{ GeV}/c^2$, where $M_{K_S^0}$ is the known mass of the K_S^0 meson [22].

C. Single-tag events

The ST D^\pm mesons are reconstructed in the six ST hadronic-decay modes and separated from background using two variables: the energy difference $\Delta E = E_D - E_{\text{beam}}$ and the beam constrained mass $M_{\text{BC}} = \sqrt{E_{\text{beam}} - p_D^2}$, where E_{beam} is beam energy, E_D and p_D are the energy and momentum of the ST D^\pm meson candidates in the rest frame of the e^+e^- system, respectively. When multiple candidates for a specific ST mode are found, the one with minimum $|\Delta E|$ is retained. The ST candidate events are further required to have ΔE within $(-55, +40)$ MeV for ST modes including a π^0 , and within $(-25, +25)$ MeV otherwise.

To determine the yields of D^\pm meson for each ST decay modes, binned maximum-likelihood fits are performed to the M_{BC} distributions in the range from 1.8365 to 1.8865 GeV/c^2 , as illustrated in Fig. 2 for the D^+ meson. In the fit, the signal is modeled by the MC-simulated shape convolved with a double-Gaussian function to

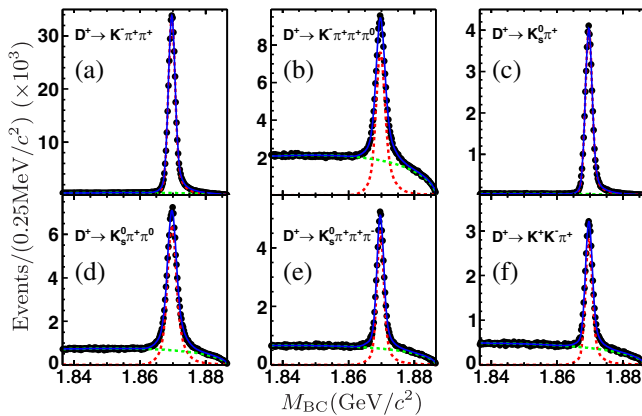


FIG. 2. M_{BC} fit in data for ST decay modes (a) $D^+ \rightarrow K^- \pi^+ \pi^+$, (b) $D^+ \rightarrow K^- \pi^+ \pi^+ \pi^0$, (c) $D^+ \rightarrow K_S^0 \pi^+$, (d) $D^+ \rightarrow K_S^0 \pi^+ \pi^0$, (e) $D^+ \rightarrow K_S^0 \pi^+ \pi^+ \pi^-$, (f) $D^+ \rightarrow K^+ K^- \pi^+$. The red and green dashed lines are signal and background, respectively. The blue solid lines are the sum of signal and background. The black points are data.

TABLE I. Summary of ST yields N_{ST}^i , ST efficiencies ϵ_{ST}^i (%), and DT efficiencies $\epsilon_{\text{DT}}^{i,c1}$ and $\epsilon_{\text{DT}}^{i,c2}$ (%), for the different ST decay modes, which are used to calculate $N_{\text{ST}}^{\text{tot}}$ and ϵ_{sig} in Eq. (1). $\epsilon_{\text{DT}}^{i,c1}$ and $\epsilon_{\text{DT}}^{i,c2}$ are DT efficiencies for signal channels with $\Delta|B-L|=0$ and $\Delta|B-L|=2$, respectively.

ST modes	$N_{\text{ST}}^i (\times 10^3)$	ϵ_{ST}^i	$\epsilon_{\text{DT}}^{i,c1}$	$\epsilon_{\text{DT}}^{i,c2}$
$D^+ \rightarrow K^- \pi^+ \pi^+$	390.2 ± 1.1	50.22 ± 0.03	9.79	9.26
$D^+ \rightarrow K^- \pi^+ \pi^+ \pi^0$	124.0 ± 0.6	26.40 ± 0.05	5.51	5.21
$D^+ \rightarrow K_S^0 \pi^+$	45.9 ± 0.2	50.58 ± 0.10	9.69	9.17
$D^+ \rightarrow K_S^0 \pi^+ \pi^0$	106.7 ± 0.6	27.07 ± 0.06	5.66	5.36
$D^+ \rightarrow K_S^0 \pi^+ \pi^+ \pi^-$	56.9 ± 0.4	28.16 ± 0.08	5.64	5.34
$D^+ \rightarrow K^+ K^- \pi^+$	34.6 ± 0.3	41.13 ± 0.15	7.88	7.46
$D^- \rightarrow K^+ \pi^- \pi^-$	392.4 ± 0.7	51.19 ± 0.03	9.21	9.72
$D^- \rightarrow K^+ \pi^- \pi^- \pi^0$	127.7 ± 1.0	26.86 ± 0.06	5.19	5.47
$D^- \rightarrow K_S^0 \pi^-$	45.5 ± 0.2	50.64 ± 0.09	9.12	9.62
$D^- \rightarrow K_S^0 \pi^- \pi^0$	107.6 ± 0.6	27.21 ± 0.05	5.33	5.63
$D^- \rightarrow K_S^0 \pi^- \pi^- \pi^+$	56.2 ± 0.4	27.87 ± 0.07	5.31	5.60
$D^- \rightarrow K^+ K^- \pi^-$	34.6 ± 0.3	40.40 ± 0.12	7.42	7.83

take the resolution difference between data and MC simulation into account. The means and widths of the double-Gaussian function are free independent parameters in the fit. The combinatorial background is described by an ARGUS function [27]. Candidate events within $M_{\text{BC}} \in (1.863, 1.877) \text{ GeV}/c^2$ are kept for further analysis. The corresponding yields of the ST D^\pm mesons are determined by integrating the fitted signal line shape in the same M_{BC} range, as summarized in Table I. Summing over all six ST modes, the total yields $N_{\text{ST}}^{\text{tot}}$ are $(758.2 \pm 1.4) \times 10^3$ for D^+ mesons and $(763.9 \pm 1.5) \times 10^3$ for D^- mesons. The detection efficiency of ST reconstruction for the decay mode i , ϵ_{ST}^i , is obtained from fits to the corresponding M_{BC} distribution of inclusive MC samples, as summarized in Table I.

D. Double-tag events

DT signal candidates are selected from the sample of ST D^\pm events by requiring an electron candidate and no additional charged tracks in the event. A two-constraint (2C) kinematical fit is performed by imposing energy and momentum conservation, and constraining the invariant mass of ST D^\pm candidates as well as the mass of the electron-(anti)neutron system to be the known mass of D^\mp meson [22], in which the (anti)neutron is regarded as a missing particle with unknown mass. The fit is required to converge, but no further selection on the χ^2 of the fit is applied. The momentum and invariant mass of the (anti)neutron obtained from the kinematic fit ($p_{n/\bar{n}}$ and $M_{n/\bar{n}}$) are recorded for the subsequent analysis. To suppress backgrounds, candidate events are required to possess a shower in the EMC around the fitted direction of the

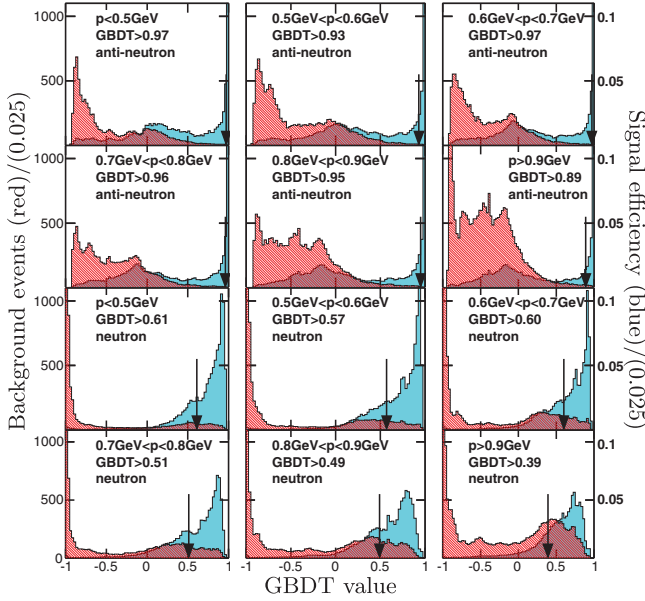


FIG. 3. The distribution of GBDT values for individual (anti)neutron momentum bins. The top six histograms are for antineutrons and the bottom six are for neutrons. The blue filled histograms are signal and the red hatched ones are backgrounds. The black arrows show the GBDT selection requirement value. The y axes on the left (right) mean B (ϵ) for background (signal) in the quantity $\epsilon/(1.5 + \sqrt{B})$.

(anti)neutron within an opening angle of 30° . If there are several showers in this region, the one with the largest energy is selected.

MC studies with a generic event-type analysis tool, TopoAna [28], indicate that the backgrounds in the selected samples are dominated by semileptonic decays of D^\pm meson with K_L^0 and π^0 mesons in the final state. Taking into account the result of the MC simulation, the selected showers in the EMC are further required to lie no more than 10° (15°) from the direction of the neutron (antineutron) candidate. In addition, a Multivariate Data Analysis (MVA) based on the shower shape in the EMC is performed based on a Gradient Boosted Decision Trees (GBDT) algorithm. The utilized variables include the total deposited energy E_{tot} , the number of hit crystals in the EMC N_{hit} , and the A20 and A42 Zernike moments as defined in Ref. [29]. In order to train and test the MVA, high-purity training and testing samples, including the (anti)neutron signal, as well as K_L^0 and photon backgrounds, are obtained from data using a selection that is independent of any EMC information. The (anti)neutron sample comes from the decay process $J/\psi \rightarrow \bar{p}n\pi^+ + \text{c.c.}$, the K_L^0 sample from $J/\psi \rightarrow K\pi K_L^0$ and the photon sample from $J/\psi \rightarrow \rho\pi^0$ with $\pi^0 \rightarrow \gamma\gamma$. Studies show that the distributions of the shower-shape variables have a significant dependence on the momentum of the (anti)neutron. Therefore, the MVA is performed in separate (anti)neutron momentum bins of width $100 \text{ MeV}/c$. For a specific (anti)neutron momentum

bin, the training and testing background samples are reweighted according to their expected momentum line shapes, which are obtained from the inclusive MC samples. The distributions of GBDT values in the different momentum bins for the antineutron and neutron as well as for the backgrounds are shown in Fig. 3. The selection on the GBDT values, optimized by maximizing the quantity $\epsilon/(1.5 + \sqrt{B})$ [30], where ϵ is the relative efficiency in the MVA signal sample and B is the number of background events normalized to match the luminosity of data in the inclusive MC sample, are applied and shown in Fig. 3.

The detection efficiencies for finding a matching shower, and for the selection on the opening angle and GBDT value are evaluated from data using the large and high-purity control sample of $J/\psi \rightarrow pn\pi$ decays. The efficiencies of finding a matching shower and for the requirement on the opening angle are studied as a function of two variables: the (anti)neutron momentum and $\cos\theta$, following the procedure described in Ref. [31]. The above efficiencies are directly applied to the signal MC sample with a sampling approach.

E. Signal extraction and fitting

The mass distributions of (anti)neutron $M_{n/\bar{n}}$ from the kinematic fit, after all selection cuts, are shown in Fig. 4 for the four decay processes, where the upper two plots are for the processes $D^+ \rightarrow \bar{n}e^+$ and $D^- \rightarrow ne^-$ with $\Delta|B - L| = 0$, and the lower two plots are for the processes $D^- \rightarrow \bar{n}e^-$ and $D^+ \rightarrow ne^+$ with $\Delta|B - L| = 2$. No obvious signal is observed. The DT detection efficiencies for the different ST modes are determined to be 18.65% for $D^+ \rightarrow \bar{n}e^+$, 19.92% for $D^- \rightarrow ne^-$, 19.68% for $D^+ \rightarrow ne^+$ and 18.85% for $D^- \rightarrow \bar{n}e^-$.

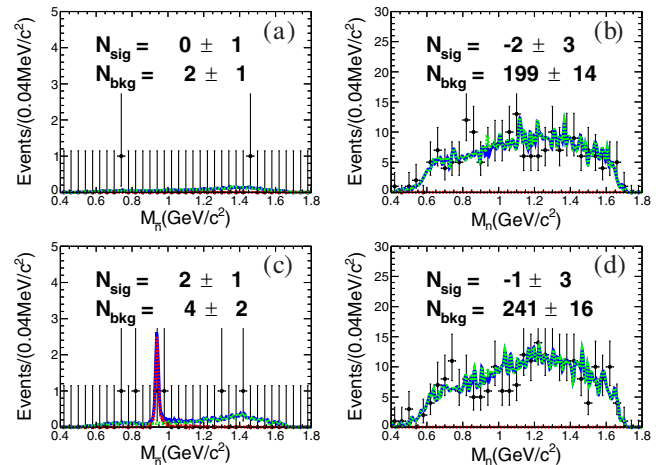


FIG. 4. Fit for $M_{n/\bar{n}}$ distributions for processes (a) $D^+ \rightarrow \bar{n}e^+$, (b) $D^- \rightarrow ne^-$, (c) $D^- \rightarrow \bar{n}e^-$, and (d) $D^+ \rightarrow ne^+$. The black dots with error bar are data. The red dotted, green dotted and blue solid lines are signal, background, and the sum of signal and background, respectively.

An unbinned maximum-likelihood fit is performed to each $M_{n/\bar{n}}$ distribution as shown in Fig. 4, individually. In the fit, signal and background are modeled by the MC-simulated shapes obtained from signal and inclusive MC samples, respectively. The yields of signal and background are left free in the fit and the returned values are shown in the plots. Since no significant signal is observed, conservative ULs are set by combining the two processes with $\Delta|B-L|=0$ and those with $\Delta|B-L|=2$, respectively, as described below.

F. Assignment of systematic uncertainties

The systematic uncertainties related to the efficiency for reconstructing the tag side cancel due to the DT method. The sources of possible systematic bias that remain include those associated with the DT-side selection efficiency, and the ST and DT yields extraction.

The uncertainties associated with the DT-side event-selection efficiency include those from the electron tracking and PID efficiencies, from the 2C kinematic fit, from the efficiency of finding a matched shower, and from requirements on the angle and the GBDT values.

The uncertainties on the tracking and PID efficiencies for electrons and positron are studied in control samples, as described in Ref. [32]. These efficiencies are studied in two-dimensional bins of momentum versus $\cos\theta$ for data and MC simulation, individually. The average relative differences on the efficiencies between data and MC simulation, which is calculated by weighting the corresponding values according to the distribution of the electron/positron signal, are assigned as the systematic uncertainties.

The uncertainty associated with the 2C kinematic fit is studied with a high-purity control sample $D \rightarrow K_S^0 \nu_e \rightarrow \pi\pi\nu_e$ decays by mimicking the $K_S^0 \nu_e$ as a missing system. The same kinematic fit is performed on this sample, and the efficiency of decays surviving this fit is measured and compared with the corresponding efficiency in MC simulation. This comparison is made as a function of the invariant mass of the $K_S^0 \nu_e$ system, and the relative difference around the neutron mass is taken as the systematic uncertainty.

The detection efficiencies for finding a matching shower and for the angle requirement in the EMC for (anti)neutron are estimated from a control sample of $J/\psi \rightarrow p n \pi$ decays in two-dimensional bins of momentum versus $\cos\theta$, and then applied directly to the signal MC samples with a sampling approach. The dominant source of potential bias from this approach arises from the different physics environment in the EMC between the signal and control sample, as well as the statistical uncertainty associated with the size of the control sample. To estimate the size of this potential bias, we compare the efficiencies between the signal MC sample and the MC-simulated control sample $J/\psi \rightarrow p n \pi$, and assign the small differences observed as

TABLE II. Summary of the systematic uncertainties on the DT efficiencies (%).

Source	$D^+ \rightarrow \bar{n}e^+$	$D^+ \rightarrow ne^+$	$D^- \rightarrow \bar{n}e^-$	$D^- \rightarrow ne^-$
e tracking	0.50	0.50	0.50	0.50
e PID	0.10	0.10	0.10	0.10
2C fit	1.00	1.00	1.00	1.00
Find shower	1.10	4.06	1.05	4.99
Angle match	2.12	1.79	2.35	1.63
GBDT cut	2.16	2.33	2.16	2.33
Total	3.41	5.14	3.54	5.85

the systematic uncertainties. The uncertainty associated with the sample size is determined by standard error propagation.

The efficiency of the requirement on the GBDT value is determined from the control sample of $J/\psi \rightarrow p n \pi$ decays in different (anti)neutron momentum bins. Two sources of potential bias are considered; background in the control sample and the choice of momentum binning. The amount of possible contamination is estimated by fitting the missing mass in the control sample in the different momentum bins, and its full effect is determined on the efficiency measurement and taken as the corresponding systematic efficiency. The possible bias associated with the momentum binning is evaluated by varying the bin size and taking the maximum change in the measured efficiency as the systematic uncertainty.

The uncertainties associated with DT selection efficiency are summarized in Table II, and the total uncertainties are the quadratic sum of the individual values.

The uncertainties on the ST yields are estimated to be 0.5% by studying the variation in results when using a different fit range of (1.8415, 1.8865) GeV/ c^2 , describing the combinatorial background with a 3-order polynomial rather than an ARGUS function, and by imposing a different endpoint of 1.8863 or 1.8867 GeV/ c^2 for the ARGUS function [33].

The uncertainty associated with the fit of the $M_{n/\bar{n}}$ distribution arises from the imperfect knowledge of the background shape and the choice of fit range, which will be considered in the determination of the upper limits.

G. Determination of the upper limits

Since no signal is observed, an UL is set on $\Delta|B-L|=0$ processes by performing a fit to the $M_{n/\bar{n}}$ distributions of $D^+ \rightarrow \bar{n}e^+$ and $D^- \rightarrow ne^-$, similar to that of Sec. III E, but with the signal yields fixed. A UL is also set on $\Delta|B-L|=2$ processes from a fit to the $D^- \rightarrow \bar{n}e^-$ and $D^+ \rightarrow ne^+$ distributions.

The fixed signal yields in the fits correspond to different branching fraction assumptions, according to the effective detection efficiencies, ST yields and the uncertainties. Likelihood values are obtained as a function of the

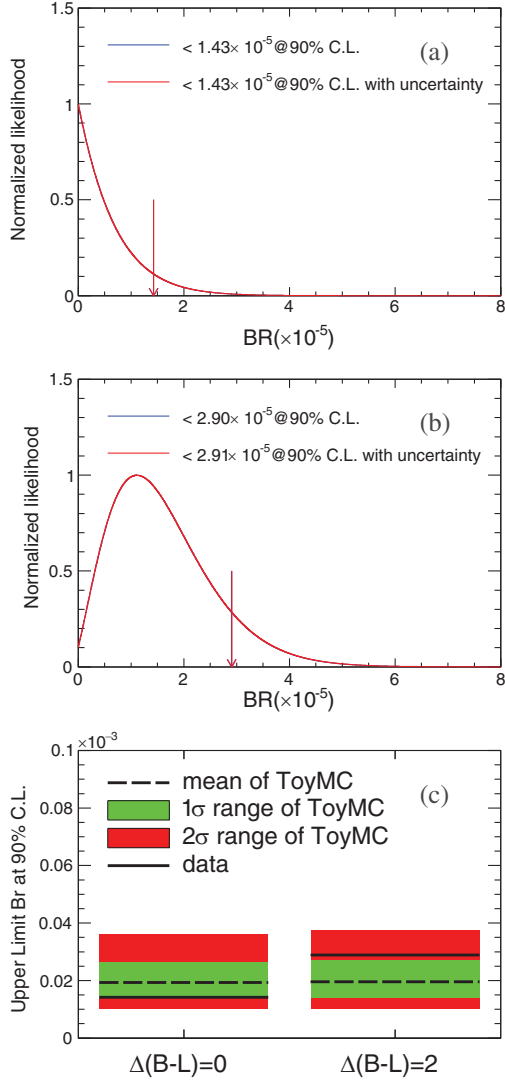


FIG. 5. Likelihood distributions and ULs results in data and Toy MC study. The top and mid figures show the likelihood distribution versus branching fraction for the processes (a) $\Delta|B-L|=0$ and (b) $\Delta|B-L|=2$. The red (blue) lines are the smeared (original) distributions. The red (blue) vertical arrows show ULs of branching fractions with (without) the systematic uncertainty included. Figure (c) shows the branching fractions of data and ToyMC studies. The black solid and dashed lines are ULs from data and means of Toy MC study, respectively. The green (red) ranges show 1(2) times of standard deviations interval in Toy MC study. The means and standard deviations are obtained by fitting the UL distribution in ToyMC samples with Gaussian function in log scale.

branching fraction, where the effects of systematic uncertainties associated with DT efficiencies and ST yields are included by convolving the likelihood distribution with Gaussian functions of mean zero and width equal to their absolute uncertainties, as described in Refs. [34]. The ULs on the branching fraction at the 90% C.L. are calculated by integrating the likelihood distribution from zero to 90% of the total curve. To take into account the effects on the

imperfect knowledge of background shape and the fit range on the $M_{n/\bar{n}}$ distributions, alternative fits are performed with different assumptions for background lineshape and fit range. The most conservative ULs obtained at the 90% C.L. are shown in Fig. 5, which are taken as the final results. These ULs are $\mathcal{B}_{D^+ \rightarrow \bar{n}e^+} < 1.43 \times 10^{-5}$ and $\mathcal{B}_{D^+ \rightarrow ne^+} < 2.91 \times 10^{-5}$. Studies of ensembles of simulated experiments ('toy MC') that contain no signal give results that are consistent with these measurements within 2σ .

IV. SUMMARY

In summary, by analyzing e^+e^- collision data with an integrated luminosity of 2.93 fb^{-1} at $\sqrt{s} = 3.773 \text{ GeV}$ taken with the BESIII detector, we search for the BNV decays $D^+ \rightarrow \bar{n}e^+$ with $\Delta|B-L|=0$ and $D^+ \rightarrow ne^+$ with $\Delta|B-L|=2$ for the first time. No signal is found and the ULs on branching fraction are determined to be $\mathcal{B}_{D^+ \rightarrow \bar{n}e^+} < 1.43 \times 10^{-5}$ and $\mathcal{B}_{D^+ \rightarrow ne^+} < 2.91 \times 10^{-5}$ for the processes with $\Delta|B-L|=0$ and $\Delta|B-L|=2$, respectively. More data at this collision energy is being collected, up to an integrated luminosity of around 20 fb^{-1} [35]. With this larger sample, and assuming no signal, it will be possible to improve the ULs by around a factor of three.

ACKNOWLEDGMENTS

The BESIII collaboration thanks the staff of BEPCII and the IHEP computing center for their strong support. This work is supported in part by National Key R&D Program of China under Contracts No. 2020YFA0406400 and No. 2020YFA0406300; National Natural Science Foundation of China (NSFC) under Contracts No. 11635010, No. 11735014, No. 11835012, No. 11935015, No. 11935016, No. 11935018, No. 11961141012, No. 12022510, No. 12025502, No. 12035009, No. 12035013, No. 12192260, No. 12192261, No. 12192262, No. 12192263, No. 12192264, No. 12192265, No. 11335008, No. 11625523, No. 11705192, No. 11950410506, No. 12061131003, No. 12105276 and No. 12122509; the Chinese Academy of Sciences (CAS) Large-Scale Scientific Facility Program; Joint Large-Scale Scientific Facility Funds of the NSFC and CAS under Contracts No. U1832207, No. U1732263, No. U1832103 and No. U2032111; CAS Key Research Program of Frontier Sciences under Contract No. QYZDJ-SSW-SLH040; 100 Talents Program of CAS; The Institute of Nuclear and Particle Physics (INPAC) and Shanghai Key Laboratory for Particle Physics and Cosmology; ERC under Contract No. 758462; European Union's Horizon 2020 research and innovation programme under Marie Skłodowska-Curie grant agreement under Contract No. 894790; German Research Foundation DFG under Contracts No. 443159800, Collaborative Research Center CRC 1044, GRK 2149; Istituto Nazionale di Fisica

Nucleare, Italy; Ministry of Development of Turkey under Contract No. DPT2006K-120470; National Science and Technology fund; National Science Research and Innovation Fund (NSRF) via the Program Management Unit for Human Resources and Institutional Development, Research and Innovation under Contract No. B16F640076; STFC (United Kingdom); Suranaree

University of Technology (SUT), Thailand Science Research and Innovation (TSRI), and National Science Research and Innovation Fund (NSRF) under Contract No. 160355; The Royal Society, UK under Contracts No. DH140054 and No. DH160214; The Swedish Research Council; U.S. Department of Energy under Contract No. DE-FG02-05ER41374.

-
- [1] A. D. Sakharov, JETP Lett. **5**, 32 (1967), http://jetpletters.ru/ps/1643/article_25089.shtml.
- [2] J. C. Pati and A. Salam, Phys. Rev. D **8**, 1240 (1973).
- [3] H. Georgi and S. L. Glashow, Phys. Rev. Lett. **32**, 438 (1974).
- [4] S. Raby, arXiv:hep-ph/0608183v1.
- [5] A. Davidson, Phys. Rev. D **20**, 776 (1979).
- [6] R. E. Marshak and R. N. Mohapatra, Phys. Lett. B **91**, 222 (1980).
- [7] S. Lola and G. G. Ross, Phys. Lett. B **314**, 336 (1993).
- [8] N. Polonsky, *Supersymmetry: Structure and Phenomena* (Springer Berlin, Heidelberg, 2001), 10.1007/3-540-44642-7.
- [9] F. Wilczek and A. Zee, Phys. Lett. B **88**, 311 (1979).
- [10] P. Rubin *et al.* (CLEO Collaboration), Phys. Rev. D **79**, 097101 (2009).
- [11] P. del Amo Sanchez *et al.* (BABAR Collaboration), Phys. Rev. D **83**, 091101 (2011).
- [12] M. E. McCracken *et al.*, Phys. Rev. D **92**, 072002 (2015).
- [13] M. Ablikim *et al.* (BESIII Collaboration), Phys. Rev. D **101**, 031102 (2020).
- [14] W. S. Hou, M. Nagashima, and A. Soddu, Phys. Rev. D **72**, 095001 (2005).
- [15] M. Ablikim *et al.* (BESIII Collaboration), Nucl. Instrum. Methods Phys. Res., Sect. A **614**, 345 (2010).
- [16] C. H. Yu *et al.*, *Proceedings of IPAC2016, Korea* (JACoW, Geneva, Switzerland, 2016).
- [17] S. Agostinelli *et al.* (GEANT4 Collaboration), Nucl. Instrum. Methods Phys. Res., Sect. A **506**, 250 (2003).
- [18] Z. Y. Deng *et al.*, High Energy Phys. Nucl. Phys. **30**, 371 (2006), <http://cpc.ihep.ac.cn/article/id/283d17c0-e8fa-4ad7-bfe3-92095466def1>.
- [19] W. D. Li *et al.*, *Proceeding of CHEP2006* (Mumbai, India, 2006).
- [20] S. Jadach, B. F. L. Ward, and Z. Was, Phys. Rev. D **63**, 113009 (2001); Comput. Phys. Commun. **130**, 260 (2000).
- [21] D. J. Lange, Nucl. Instrum. Methods Phys. Res., Sect. A **462**, 152 (2001); R. G. Ping, Chin. Phys. C **32**, 599 (2008).
- [22] P. A. Zyla *et al.* (Particle Data Group), Prog. Theor. Exp. Phys. **2020**, 083C01 (2020).
- [23] J. C. Chen, G. S. Huang, X. R. Qi, D. H. Zhang, and Y. S. Zhu, Phys. Rev. D **62**, 034003 (2000).
- [24] R. L. Yang, R. G. Ping, and H. Chen, Chin. Phys. Lett. **31**, 061301 (2014).
- [25] E. Richter-Was, Phys. Lett. B **303**, 163 (1993).
- [26] R. M. Baltrusaitis *et al.* (MARKIII Collaboration), Phys. Rev. Lett. **56**, 2140 (1986).
- [27] H. Albrecht *et al.* (ARGUS Collaboration), Phys. Lett. B **241**, 278 (1990).
- [28] X. Y. Zhou, S. X. Du, G. Li, and C. P. Shen, Comput. Phys. Commun. **258**, 107540 (2021).
- [29] R. Sinkus and T. Voss, Nucl. Instrum. Methods Phys. Res., Sect. A **391**, 360 (1997).
- [30] G. Punzi, eConf **C030908**, MODT002 (2003), <https://www.slac.stanford.edu/econf/C030908/papers/MODT002.pdf>.
- [31] L. Liu, X. R. Zhou, and H. P. Peng, Nucl. Instrum. Methods Phys. Res., Sect. A **1033**, 166672 (2022).
- [32] M. Ablikim *et al.* (BESIII Collaboration), Phys. Rev. Lett. **127**, 131801 (2021).
- [33] M. Ablikim *et al.* (BESIII Collaboration), Chin. Phys. C **40**, 113001 (2016).
- [34] K. Stenson, arXiv:physics/0605236.
- [35] M. Ablikim *et al.* (BESIII Collaboration), Chin. Phys. C **44**, 040001 (2020).